International Journal of Mechanical Sciences 85 (2014) 196–204

Contents lists available at ScienceDirect

International Journal of Mechanical Sciences

journal homepage: www.elsevier.com/locate/ijmecsci

Simulation of hot forming processes: Using cost effective micro-structural constitutive models

Reza Jafari Nedoushan [a], Mahmoud Farzin [a], Dorel Banabic [b,*]

[a] Department of Mechanical Engineering, Isfahan University of Technology, Isfahan 84156, Iran
[b] CERTETA Research Centre, Technical University of Cluj-Napoca, 28 Memorandumului, 400114 Cluj-Napoca, Romania

ARTICLE INFO

Article history:
Received 22 April 2012
Received in revised form
27 December 2012
Accepted 26 April 2014
Available online 15 May 2014

Keywords:
Hot metal forming
Constitutive equations
Grain boundary mechanisms
Grain growth hardening

ABSTRACT

Constitutive models for dominant mechanisms in hot forming are proposed. These models consider inter-granular deformation, grain boundary sliding, grain boundary diffusion and grain growth. New stress–strain rate relationships are proposed to predict deformation due to grain boundary sliding and grain boundary diffusion. Besides a Taylor type polycrystalline constitutive model, a visco-plastic relation in conjunction with two different yield functions is used to predict inter-granular deformation. Step strain rate tests and bulge forming test are simulated with the proposed models. Results are compared with experimental data to verify the constitutive models. It is concluded that the visco-plastic models can predict material behavior in hot deformations as accurately as the polycrystalline model but with much less computational costs. To examine the hardening effects, the model is calibrated with tensile test data of AA5083 at 550 °C, where hardening is remarkable. Then, as an example, it is used to simulate a tray forming experiment. Dome heights and tray thicknesses at various positions during forming process are very close to experimental observations.

1. Introduction

Sheet metal components with complex shapes can be made at elevated temperatures by superplastic forming (SPF) and quick plastic forming (QPF). Finite element simulation has reduced the number of trial forming experiments in these processes. The accuracy of a constitutive model is currently the most significant issue to achieve useful predictions in FE simulations of these processes.

The microstructure of a hot formed metal differs strikingly from that of a part formed at room temperature. The difference is more evident in superplastic forming, and the deformation mechanisms differ substantially from cold forming [1]. Several mechanisms may play some roles in hot forming including dislocation movement inside grains, grain boundary sliding, grain boundary diffusion, and grain boundary migration. Various micro-structural constitutive models were proposed for better understanding of these mechanisms and/or exact prediction of material behavior [1–5]. Contributions of grain boundary sliding and grain boundary diffusion in total deformation have been considered by many researchers [1,3,6–10].

Some researchers investigated grain growth during hot deformation [11–16] and a few models were also proposed to predict grain growth [14,15,17–19]. These models have been numerously used in simulations of superplastic forming [20–23].

The previous works on hot forming constitutive equations can be generally classified into two groups:

a. Macro-constitutive equations that can be used at every material point to predict material macro-behavior in complex processes [23,24]. Norton Half behavior is an example of these constitutive models [25]. These types of constitutive models that include material dependency of strain rate and grain size are applicable for limited conditions of forming. For example some of these relations can explain material constitutive behavior when logarithmic scale of stress and strain rate diagram is a straight line. Some other relations can only be used for certain grain sizes that material shows superplastic behavior.
b. Micro-constitutive models that consider micro-structure of material for better understanding of deformation mechanisms [2–5]. This group can predict material behavior in various microstructures and strain rates after calibration with fewer experiments. However these micro-constitutive models cannot directly be used in simulation of complicated processes due to high computational costs and usually a multi-scale modeling is required for this purpose [26].

* Corresponding author.

http://dx.doi.org/10.1016/j.ijmecsci.2014.04.026
0020-7403/

The aim of the current work is to propose micro-constitutive models that can be calibrated with a few experiments, the same as group (b) but can be directly used to predict material behavior in macro-scale simulation of complicated processes, the same as group (a). These models are expected to properly predict material behavior for a vast range of grain sizes, strain rates and strains similar to group (b) but with much less computational costs.

To prepare the models in this paper, material deformation is divided into two sections: inter-granular and grain boundary mechanisms. Grain boundary mechanisms include: grain boundary sliding (GBS), grain boundary diffusion (GBD) and grain growth. New micro-constitutive relationships are proposed for GBS and GBD that correlate macro-stresses to strain rates. These relationships have been previously verified for various strain rates, grain sizes and stress states [27] but grain growth and consequent hardening were not considered in these relationships. In the other words in this model dependency of material on strain is ignored. To add this missing part to these relationships a grain growth model that was proposed by Kim et al. [17] is also used beside these relationships to consider grain size evolution under deformation.

Besides the above mentioned boundary mechanisms, inter-granular deformation is also predicted by three different approaches I: the Taylor type polycrystalline approach, II: Von-Mises viscoplastic model and III: J2-J3 viscoplastic model.

It should be mentioned that initial texture or texture development during deformation causes material anisotropic behavior in cold forming [28–30]. The Taylor type polycrystalline approach is widely used to predict macro-material behavior in cold forming processes especially when material anisotropy due to material texture is a crucial issue [31–36]. In hot forming, especially superplastic forming in contrast with cold forming, texture will reduce as the material undergoes deformation [1] and in this work it is supposed that material have an isotropic behavior. The two above mentioned macro-viscoplastic models are proposed to have the same behavior with the Taylor type polycrystalline model without considering texture for various strain rates and stress states, but with much less computational costs. The above mentioned models are compared with each other in different simulations. The remainder of this paper is organized as follows: At first, assumptions and governing equations are listed for the mechanisms and models. Then step strain rate tests and gas pressure forming are simulated to show the ability and limitations of the various models. Finally, one of the viscoplastic models is used in the circumstances that grain growth has a significant role. For this purpose, the model is calibrated with tensile test data at different strain rates and then the model is used to simulate gas pressure tray forming.

In summary it will be shown that the proposed boundary micro-constitutive models in conjunction with inter-granular viscoplastic models can be used in various hot forming conditions such as temperatures, strain rates, strains and stress states in a very cost effective and accurate manner.

2. Model description

In the proposed model a material point is visualized as a representative of grains and their boundaries. So the macroscopic deformation is a result of inter-granular deformation caused by dislocations creep, GBS and GBD, at that point:

$$L_{ij} = L_{ij}^{CR} + L_{ij}^{GBS} + L_{ij}^{GBD} \tag{1}$$

where L_{ij} denotes the total velocity gradient tensor; L_{ij}^{CR} is the velocity gradient due to inter-granular deformation; L_{ij}^{GBS} is the velocity gradient due to GBS; L_{ij}^{GBD} is the GBD velocity gradient.

2.1. Inter-granular deformation

At first, a standard crystal plasticity model with the Taylor type polycrystalline approach is used to approximate the response of material within the grains. Then a viscoplastic relation in conjunction with two suitable yield functions is proposed to be substituted and compared with Taylor type polycrystalline model. Here the objective is to find a cost effective and accurate constitutive model which represents the inter-granular material behavior.

2.1.1. Polycrystalline constitutive model

The crystal plasticity model, used in this work employs the framework of classical crystal plasticity by Peirce and Asaro [37,38] and Asaro [39,40]. Implementation of this model is based on the user-material routine (UMAT) of Huang [41] in the environment of ABAQUS finite element code. In this paper, the grains are all face-centered cubic (FCC) crystals, with twelve (111) [110] slip systems.

The velocity gradient tensor is decomposed into elastic and plastic parts as:

$$L_{ij}^{CR} = L_{ij}^{e} + L_{ij}^{p} \tag{2}$$

The symmetric and anti-symmetric parts of velocity gradient tensor can also be decomposed into elastic and plastic parts

$$D_{ij}^{CR} = D_{ij}^{e} + D_{ij}^{p} \tag{3-1}$$

$$W_{ij}^{CR} = W_{ij}^{e} + W_{ij}^{p} \tag{3-2}$$

Note that D_{ij}^{e} is related to stress rate through the usual linear elastic constitutive equations. D_{ij}^{p} and W_{ij}^{p} are computed by summing the shearing rates of the active slip systems

$$D_{ij}^{p} = \frac{1}{2}\sum_{\alpha=1}^{N} \dot{\gamma}^{\alpha}(s_i^{\alpha} m_j^{\alpha} + s_j^{\alpha} m_i^{\alpha}) \tag{4-1}$$

$$W_{ij}^{p} = \frac{1}{2}\sum_{\alpha=1}^{N} \dot{\gamma}^{\alpha}(s_i^{\alpha} m_j^{\alpha} - s_j^{\alpha} m_i^{\alpha}) \tag{4-2}$$

where s_i^{α} and m_i^{α} denote, the components of unit vectors parallel to the slip direction and slip plane normal respectively, and $\dot{\gamma}^{\alpha}$ is the shear rate on slip systemα and is computed from:

$$\dot{\gamma}^{\alpha} = \dot{\gamma}_0^{\alpha}\left(\frac{\tau^{\alpha}}{\tau_0}\right)^{n_c} \tag{5}$$

here, $\dot{\gamma}_0^{\alpha}$ is a characteristic slip rate; k is the stress exponent of the slip system; and τ_0 is characteristic flow strength. Hardening is neglected in inter-granular computations and τ_0 is assumed to be constant. τ^{α} is the resolved shear stress on the slip system α.

For polycrystalline materials, a material point can be visualized as a multitude of single crystals, and the constitutive response at this material point is taken as a suitable average of the constitutive response of the individual crystals comprising this representative point. In the present work, the Taylor type model [42] is used to calculate the crystal or inter-granular deformation. In this model the deformation in each grain is taken to be identical to the macroscopic deformation of the continuum. Furthermore, the macroscopic values of all quantities, such as stresses, stress rates and elastic modules, are obtained by averaging their respective values over grains with random orientations at that particular material point.

2.1.2. Viscoplastic models

In this section two viscoplastic constitutive models are used which represent the same inter-granular deformation as polycrystalline model with the objective of reducing computational costs. These models are defined to predict the same behavior as polycrystalline materials in various strain rates and stress states.

2.1.2.1. Strain rate. To investigate effect of strain rate in FCC polycrystalline material, various strain rates are applied to this material in simple tension. The simple tension is modeled in ABAQUS FEM code as discussed in Ref. [27]. It should be emphasized that grain boundary mechanisms are ignored here and only inter-granular deformation is considered. For this purpose Taylor type polycrystalline model is implemented in ABAQUS code through a user defined material subroutine (UMAT). The parameters that are used in these simulations are shown in Table 1.

Fig. 1 shows flow stress–strain rate relationship. The relation is exactly a straight line in a logarithmic scale; therefore the following viscoplastic equation can be proposed to relate effective plastic strain rate and equivalent stress:

$$\sigma_e = A\dot{\varepsilon}_{eff}^{pB} \tag{6}$$

where A and B are material constants and are $A=124.0$ and $B=0.23$ in this case. σ_e will be calculate by yield function proposed in next section.

2.1.2.2. Stress state. The polycrystalline behavior is also examined in various stress states. For this purpose, the material is subjected to 2D tension and compression tests with deferent stress ratios to obtain polycrystalline yield locus. The applied boundary condition in this case is explained in [27]. Fig. 2 shows the resulted yield locus and its comparison with Tresca and Von-Mises yield loci. As it can be seen in this figure the polycrystalline yield locus is located between Tresca and Von-Mises yield loci and is closer to Von-Mises criterion. Therefore Von-Mises criterion can be used to predict FCC polycrystalline behavior in various stress states. The following yield function is also proposed to predict polycrystalline behavior more closely:

$$f = J_2^3 - \phi J_3^2 - Y^6 = 0 \tag{7}$$

Table 1
Parameters used in the simple tension simulation of FCC polycrystalline.

Parameter	Value
Young's modulus (E)	70,000 MPa
Poisson's ratio (ν)	0.3
Characteristic strain rate ($\dot{\gamma}_0$)	6 s^{-1}
Slip system strength (τ_0)	65 MPa
Stress exponent of slip (n_c)	4.35

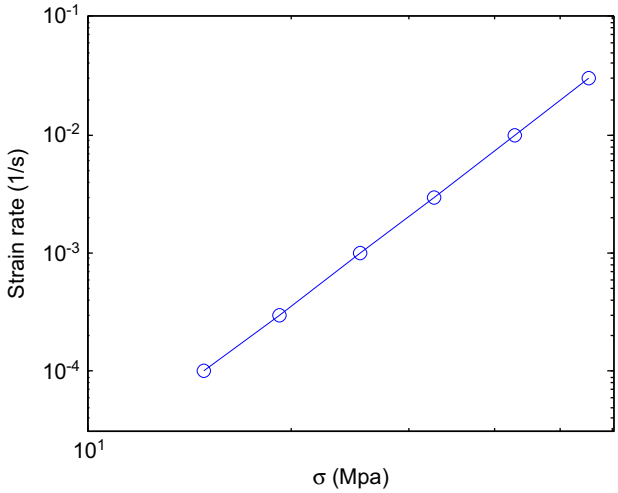

Fig. 1. Flow stress vs. strain rate for Taylor type FCC polycrystalline.

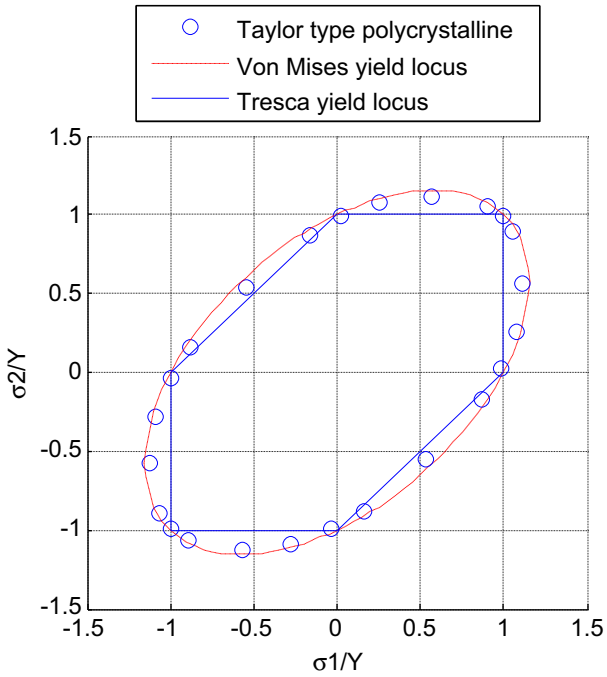

Fig. 2. Resulting yield loci from the Taylor type polycrystalline and also Tresca and Von-Mises yield functions.

where J_2 and J_3 are second and third invariants of deviatoric stress tensor, Y is strain dependent yield stress and ϕ is material constants. When ϕ is 1.5 the best agreement between polycrystalline yield locus and the proposed J2-J3 yield locus will be obtained.

Now polycrystalline behavior can be switched with Eq. (6) and one of the above mentioned yield functions. Although effects of strain rate and stress state were considered separately but the resulted model behave similar to polycrystalline model in any combination of strain rates and stress states. To confirm this fact, resulting yield loci from polycrystalline and J2-J3 models are compared for various strain rates in Fig. 3.

2.2. Grain boundary sliding

Grain boundary sliding occurs due to shear tractions acting tangent to the grain boundary. For calculating GBS deformation in a material point it is assumed that:

a. The boundaries are comprised of parallel planes in several presumed directions at a material point. So a set of normal vectors indicates the boundaries.
b. Stress tensor is identical for all boundaries and is equal to macro-stress tensor in a material point. This assumption means that grain boundary sliding will be calculated with the average stress applied to the entire boundaries in a material point.
c. Relative sliding velocity between two grains has the same direction with shear traction acting on the boundary.

Shear traction acting on all parallel boundaries with a normal vector n_i^β can be calculated as follows:

$$\tau_i^\beta = \sigma_{ij} n_j^\beta - (\sigma_{mj} n_m^\beta n_j^\beta) n_i^\beta = \sigma_t^\beta t_i^\beta \tag{8}$$

The superscript β indicates the number of assumed boundary planes. Here σ_t^β is the resolved shear stress and t_i^β is direction of this shear traction. If the resolved shear stress in these boundaries is greater than a threshold stress σ_{th}, the following viscous

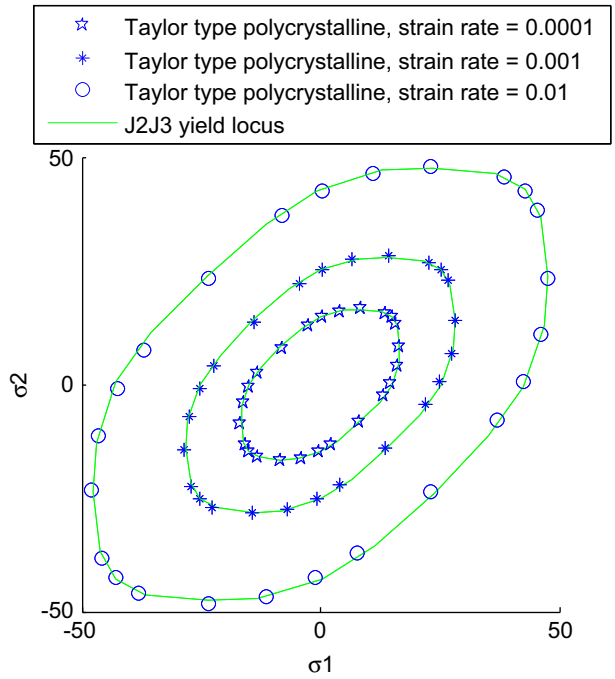

Fig. 3. Resulting yield loci from a Taylor type polycrystalline and J2-J3 yield function in various strain rates.

constitutive equation is assumed to characterize sliding. This equation relates the relative sliding velocity of two adjacent grains to the resolved shear stress [3,5]

$$\begin{cases} v_t^\beta = \frac{\Omega\eta\exp(-Q_{GBS}/kT)}{kT}\left(\frac{\sigma_t^\beta-\sigma_{th}}{\sigma_{th}}\right)^{n_1} & \text{if} \quad \sigma_t^\beta > \sigma_{th} \\ v_t^\beta = 0 & \text{if} \quad \sigma_t^\beta < \sigma_{th} \end{cases} \tag{9}$$

here, η is a characteristic sliding velocity; k is the Boltzmann constant; T is the absolute temperature; n_1 is the stress exponent of the slid; Ω is the atomic volume and Q_{GBS} is the activation energy for GBS. Shear strain rate due to GBS in all parallel boundary planes with a normal vector n_i^β can be written as:

$$\dot{\gamma}^\beta = \frac{v_t^\beta}{d} \tag{10}$$

where, d is the average grain size. The macro-deformation due to GBS in these parallel boundaries can be written as:

$$D_{ij}^\beta = \frac{1}{2}\dot{\gamma}^\beta(n_i^\beta t_j^\beta + t_i^\beta n_j^\beta) \tag{11-1}$$

$$W_{ij}^\beta = \frac{1}{2}\dot{\gamma}^\beta(n_i^\beta t_j^\beta - t_i^\beta n_j^\beta) \tag{11-2}$$

Considering all boundaries:

$$D_{ij}^{GBS} = \frac{1}{2}\sum_{\beta=1}^{N_b}\dot{\gamma}^\beta(n_i^\beta t_j^\beta + t_i^\beta n_j^\beta) \tag{12-1}$$

$$W_{ij}^{GBS} = \frac{1}{2}\sum_{\beta=1}^{N_b}\dot{\gamma}^\beta(n_i^\beta t_j^\beta - t_i^\beta n_j^\beta) \tag{12-2}$$

where N_b is the number of assumed boundary.

2.3. Grain boundary diffusion

Atoms (or equivalently, vacancies) adjacent to the grain boundary are assumed to be mobile. Atoms may detach from each grain, diffuse along the boundary, and then re-attach to one of the two adjacent grains [3]. In this process, atoms detach from regions of the grain boundary that are subjected to compressive stress and migrate to regions that are under tensile stress [3,5]. Hence grain-boundary diffusion is assumed to be a function of variation of the normal stress acting on the boundary. Therefore it is assumed that the flux of atoms tangent to each interface is related to the normal stress [3,5] through:

$$j = -\frac{\Omega D_{GBt}\delta_{GB}\exp(-Q_{GBt}/kT)}{2kT}\frac{\partial\sigma_n}{\partial s} \tag{13}$$

where T is absolute temperature; k is Boltzmann constant; $D_{GBt}\exp(-Q_{GBt}/kT)$ is the tangential grain boundary diffusivity; Q_{GBt} is the corresponding activation energy; $\delta_{GB}/2$ is the thickness of the diffusion layer in one grain. When temperature is constant, Eq. (13) can be simplified to:

$$j = -q\frac{\partial\sigma_n}{\partial s} \tag{14}$$

where q is a constant.

Remembering that a material point was visualized as an aggregate of grains with their boundaries, for calculating GBD deformation it is assumed that:

a. Deformation caused by GBD in a material point can be replaced by deformation that occurs in one grain by GBD. With this assumption atoms only move around one grain and cannot move from one grain to another one and grain boundary migration is not modeled. With this assumption grain boundaries cannot exchange atoms at triple junctions and satisfaction of mass conservation at triple junctions does not need to be considered.
b. The grain has a spherical shape.
c. Stress is constant around the grain boundary and equals to macro-stress at that material point.

With these assumptions, a grain boundary is a two-dimensional space (spherical surface) and Eq. (14) is extended for a two dimensional space:

$$\vec{j} = -q\vec{\nabla}\sigma_n = -q\left(\frac{\partial\sigma_n}{\partial s_1}e_1 + \frac{\partial\sigma_n}{\partial s_2}e_2\right) \tag{15}$$

where e_1 and e_2 are unit base vectors on the boundary which is a two dimensional space; s_1 and s_2 are lengths along e_1 and e_2. Considering mass conservation, the velocity discontinuity in the direction of the normal to the grain boundary is:

$$[v_n] = -q\left(\frac{\partial^2\sigma_n}{\partial s_1^2} + \frac{\partial^2\sigma_n}{\partial s_2^2}\right) \tag{16}$$

It can be proved from the above equation that in GBD mechanism, rate of deformation tensor and deviatoric stress tensor relate via [27]:

$$D_{ij}^{GBD} = \frac{1.6755K}{d^3}S_{ij} \tag{17}$$

where K is a constant.

2.4. Grain growth model

Eqs. (10) and (17) show that grain size is effective in stress–strain rate relationship in GBS and GBD mechanisms respectively. Therefore in order to determine the flow stress, it is necessary to know the current grain size. In hot deformation the grain size will be changed by both static and deformation enhanced grain growth. Static grain growth was observed to be small for materials and temperatures under consideration [43]. There are several models proposed to describe deformation enhanced grain growth. In the current work the following model that was proposed by Kim

et al. [17] is used to predict grain size evolution during hot deformation. This model was derived considering a micro-structural approach.

$$\dot{d} = C d\dot{\varepsilon}^{p}_{eff} \tag{18}$$

where $\dot{d}$, is the dynamic grain growth rate and C is an assumed constant. According to Eqs. (10) and (17), for a given deformation rate as the grain size increases the flow stress also increases. Therefore when the grain growth is considered in the proposed model, the hardening behavior in hot deformation can be predicted.

In summary, to predict material behavior in this paper, grain growth and deformation due to grain boundary mechanisms are computed according to the above mentioned models in all simulations but inter-granular deformation is computed with the following three approaches:

a. Using Taylor type polycrystalline (Model I).
b. Using Eq. (6) in conjunction with Von-Mises yield function (Model II).
c. Using Eq. (6) in conjunction with the J2J3 yield function as is proposed by Eq. (7) (Model III).

3. Numerical implementation

To add the proposed constitutive models to the Abaqus FEM code, a user subroutine UMAT is used. In this subroutine following algorithm shown in Fig. 4 is used. In this algorithm $d\varepsilon^{t}_{ij}$ is total strain increment; $d\varepsilon^{GBD}_{ij}$ is strain increment due to GBD; $d\varepsilon^{GBS}_{ij}$ is GBS strain increment; $d\varepsilon^{Cr}_{ij}$ is strain increment due to inter-granular deformation. $\partial\Delta\sigma/\partial\Delta\varepsilon^{Cr}$ is the Jacobean and is calculated from the Taylor model and it can be easily shown that is equal to $\partial\Delta\sigma/\partial\Delta\varepsilon^{t}$ which is the total Jacobean. θ is a character that shows GBS and GBD are calculated from the stress at the beginning or the end of the increment. For example, if $\theta = 0$, GBS and GBD are calculated from the stress value at the beginning of the increment and if $\theta = 1$, the stress value at the end of the increment will be used. In this work $\theta = 0.5$ has been used.

4. Applications and results

In this section, the proposed models are used in various strain rates and stress states to investigate the capability and limitations of these models. Then Model II is used in a situation that grain growth and hardening are also effective and predictions are compared with tray forming experiments.

4.1. Simulation of step strain-rate tensile tests

Step strain-rate tensile tests use a series of strain rates imposed upon a single specimen, to obtain data for flow stress as a function of temperature, grain size and strain rate. Further details of the step strain-rate testing procedure are described in Ref. [2,26]. The flow stress vs. strain rate data on AA5083 for six different microstructures, derived from the step strain-rate testing procedure due to Krajewski et al. [26] will be used for comparison with the predicted results in this paper.

Step strain-rate tensile test is simulated in ABAQUS FEM code with a cubic specimen with a length of a and boundary conditions that are described in Ref. [27]. The proposed models are implemented in this code through user-material routines (UMAT).

The constitutive parameters used in these simulations were calibrated with the grain sizes of 7 μm and 81.7 μm. The procedure of finding the best set of constitutive parameters for Model I is reported in Ref. [27]. For models II and III the procedure is much simpler. For these models a one dimensional code is written in MATLAB software by using Eqs. (6), (8)–(12) and (17). Then the best set of parameters obtained with this code with minimizing error between predicted stress and stress from experiments. In fact one of the advantages of models II and III is that finding their parameters is much simpler. Tables 2 and 3 show calculated parameters.

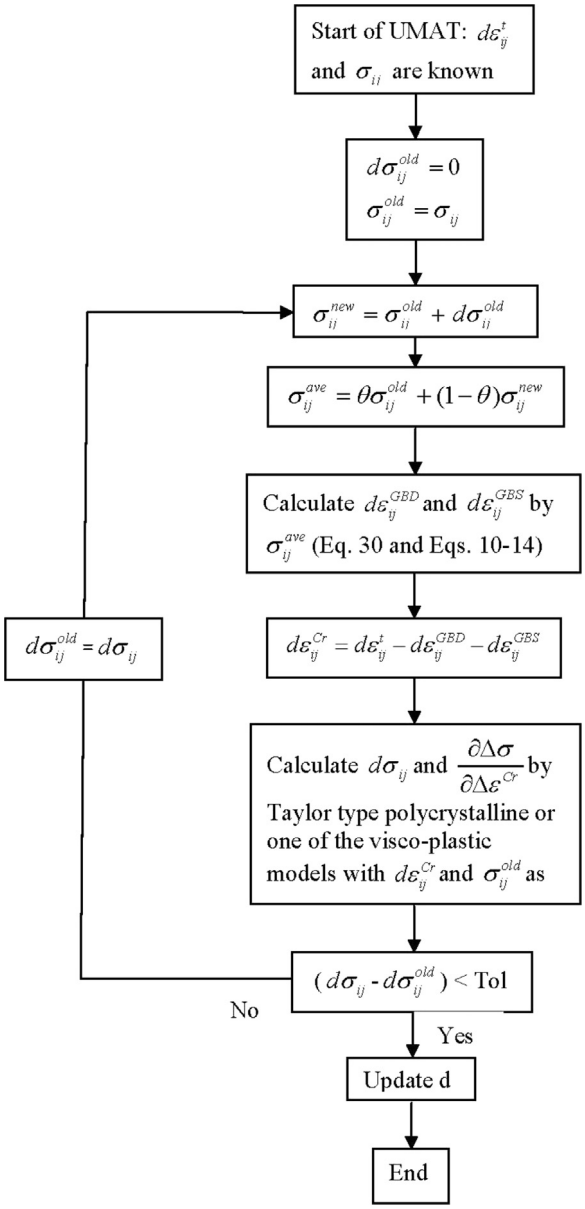

Fig. 4. Numerical algorithm used to implement constitutive equations in Abaqus software.

For this material strain hardening, which is typically associated with grain growth during hot forming, was observed to be small over the temperature, strains and strain rates under consideration [44]. Therefore the grain growth coefficient was set to be zero in these cases. The calibrated material properties were then used to predict the behavior of specimens with other grain sizes. Predictions of the three proposed models are identical as are compared with Krajewski et al. [26] results, in Fig. 5. It can be seen from this figure that the proposed models predict material behavior for various grain sizes and strain rates close to experimental data. It is worth mentioning that the three proposed models can compute contribution of each deformation mechanisms in total deformation as it is shown in [27].

Table 2
Calibrated parameters used in the present simulations for model I.

Parameter	Value
Young's modulus (E)	70,000 Mpa
Poisson's ratio (ν)	0.3
Shear modulus (μ)	26,900 Mpa
Characteristic strain rate ($\dot{\gamma}_0$)	6 s^{-1}
Slip system strength (τ_0)	65 Mpa
Stress exponent of slip (n_c)	4.35
Stress exponent of boundary slid (n)	3.6
Grain boundary sliding pre-exponential (η)	1.5e-9 mm s^{-1}
Grain growth coefficient (C)	0
Grain boundary diffusion coefficient (K)	1.34 e−11 J
Threshold stress of boundary slid (σ_{th})	0.2 MPa

Table 3
Calibrated parameters used in the present simulations for models II & III.

Parameter	Value
Young's modulus (E)	70,000 Mpa
Poisson's ratio (ν)	0.3
Shear modulus (μ)	26,900 Mpa
Strain coefficient of inter-granular deformation (A)	124.0
Stress exponent of inter-granular deformation (B)	0.23
Stress exponent of boundary slid (n)	3.6
Grain boundary sliding pre-exponential (η)	1.5e-9 mms^{-1}
Grain growth coefficient (C)	0
Grain boundary diffusion coefficient (K)	1.34 e-11 J
Threshold stress of boundary slid (σ_{th})	0.2 MPa

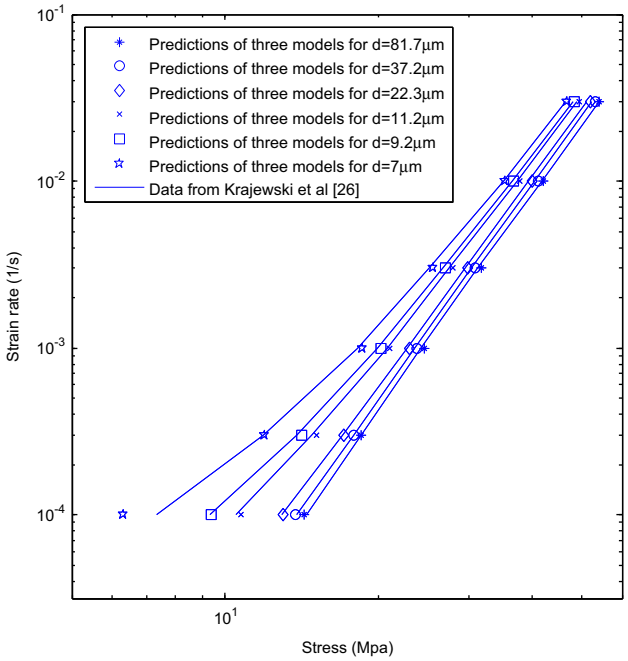

Fig. 5. Comparison of current predictions with Krajewski et al. results [26].

4.2. Gas pressure forming simulation

The material models are implemented in FEM simulations of gas-pressure bulge-forming to compare the models in situations where multidirectional stress exists. In gas-pressure bulge-forming process, the sheet is clamped between two dies and it is formed by gas pressure at a hot temperature. Details of this procedure are reported in Refs. [26,45].

In current simulations initial sheet thickness is 1.04 mm and the gas pressure is 0.25 Mpa. The considered material is AA5083 at 450 °C and hence the calibrated parameters in Tables 2 and 3 are used again.

ABAQUS STANDARD is used to simulate gas-pressure bulge-forming. The material models are applied through user subroutines. The process is considered to be axisymmetric. A mesh sensitivity study is conducted to assure that element size is sufficiently fine to provide repeatable predictions of bulge displacements and strain rates. Fig. 6 shows initial mesh of the blank, with 160 quadrilateral CAX4 elements. The implicit formulation in Abacus requires calculation of an initial elastic response; hence a linear ramp type pressure is applied within one second and is then kept constant until 1800 s. Plastic deformation was subsequently calculated for the duration of the simulations. It should be emphasized that all simulations have the same circumstances except the inter-granular constitutive models. Fig. 7 shows the deformed sheet predicted by the model II.

Fig. 8 compares predicted dome heights during forming time for the three proposed inter-granular models. Results of model I was previously compared with experimental data and good agreements obtained [27]. As it can be seen in this figure, prediction of model III is very close to model I but model II predicts dome height a little less than the other two. By comparing the inter-granular yield loci for the three models that are shown in Fig. 2, this difference is reasonable. In gas pressure forming, stress state locates between plane strain and biaxial tension. Von-Mises criterion predicts higher flow stresses than the others in this zone so the predicted displacements by this model are expected to be less.

A remarkable difference between the three proposed models is the computational costs that causes model II and III to be more attractive than model I. For the same circumstances used in different simulations, model II and III were performed about fifty times faster than model I.

4.3. Simulation of superplastic tray forming

In this section, model II is examined in a situation that grain growth has a significant effect. In hot forming processes besides initial grain size and strain rate, flow stress is also usually affected by grain size evolution and growth. In the previous sections it was shown that the model can well predict material behavior for various grain sizes and strain rates. If the model can also properly predict

Fig. 6. Initial mesh of the blank, with 160 quadrilateral CAX4 elements.

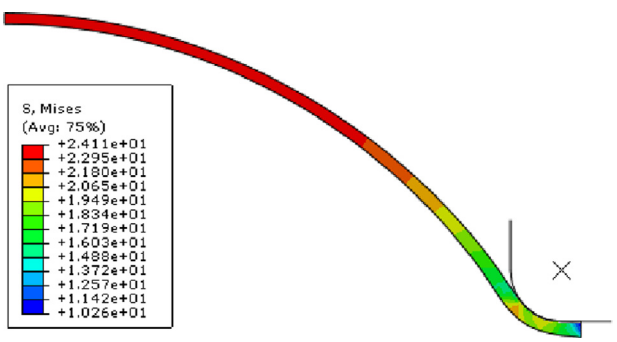

Fig. 7. Final deformed sheet predicted by model II after 1800 s. and applying a constant pressure of 0.25 MPa.

effects of hardening due to grain growth, obviously it can be used in most hot forming simulations. At first the model is calibrated by tensile tests with different strain rates and then it is used to simulate superplastic gas pressure tray forming.

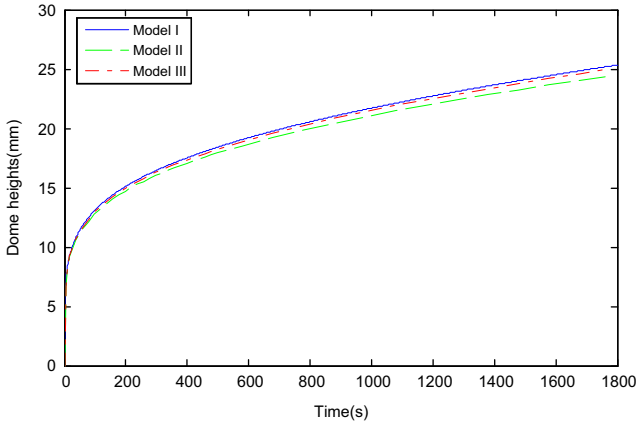

Fig. 8. Predictions of dome heights vs. time for the three models.

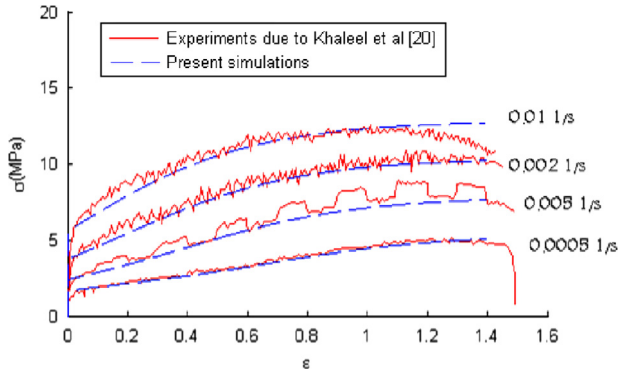

Fig. 9. Stress–strain curves on AA5083 at a constant test temperature of 550 °C.

Table 4
Parameters of model II, calibrated by tensile test curves with different stain rates.

Parameter	Value
Young's modulus (E)	67,400 Mpa
Poisson's ratio (ν)	0.3
Initial grain size d	8.6 μm
Strain coefficient of inter-granular deformation (A)	90.0
Stress exponent of inter-granular deformation (B)	0.303
Stress exponent of boundary slide (n)	1.3
Grain boundary sliding pre-exponential (η)	1.4e-5 mms – 1
Grain growth coefficient (C)	2.75
Grain boundary diffusion coefficient (K)	5.0 e-11 J
Threshold stress of boundary slide (σ_{th})	0.45 MPa

Fig. 9 shows the stress–strain relations under various strain rates for AA5083 at a constant test temperature of 550 °C [20]. Further details about composition of this material and its experimental stress–strain results have been reported by Khaleel et al. [20].

As it can be seen in Fig. 9, hardening is remarkable in this case. These curves were used to calibrate the model and calibrated parameters are shown in Table 4. These parameters were obtained from the initial yield points for four strain rates and slope of one of the curves. As it can be seen from Fig. 9, the calibrated model closely fits the experimental data for various strain rates and strains. These results, shows the ability of model to predict hardening behavior for different strain rates.

In gas pressure tray forming, a sheet is clamped on a die with a rectangular cavity of 50.8 mm width, 203 mm length, and 25.4 mm depth. Fig. 10 shows one-quarter of the die surface and the sheet. A flat flange is surrounding the cavity with 38 mm width. A die entrance radius of 3.2 mm makes the transition from the flange to the rectangular cavity.

ABAQUS EXPLICIT finite element code is used for these simulations. The sheet is meshed with 1463 quadrilateral M3D4R elements and the die has 3713 R3D4 elements. The gas pressure history used in Khaleel et al. [20] experiments, is shown in Fig. 11. In the current simulation, this pressure history is applied on the sheet by a user amplitude routine (VUAMP). The constitutive model is also implemented through a user defined material routine (VUMAT). Effect of friction coefficient on the accuracy of results is discussed by Khaleel et al. [20] and in this work the suggested friction coefficient by them is used.

In this process, the center of the sheet moves towards the bottom of the die. After a while this point contacts the die and remains fixed. Then deformation at the corners increases. Fig. 12 shows the predicted and measured depth of the center vs. time. As it can be

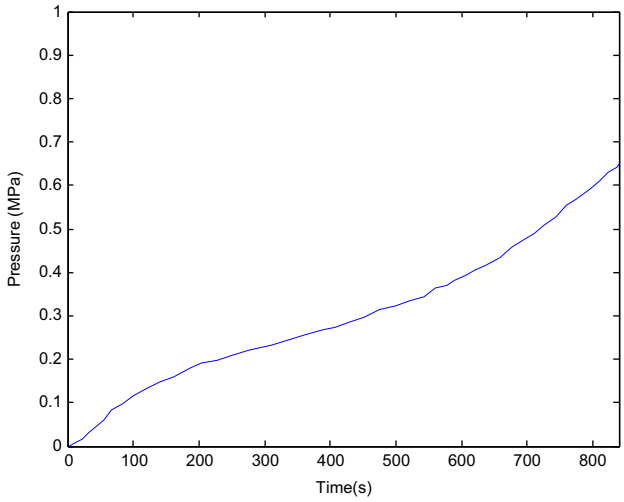

Fig. 11. Gas pressure history that was used in experiments.

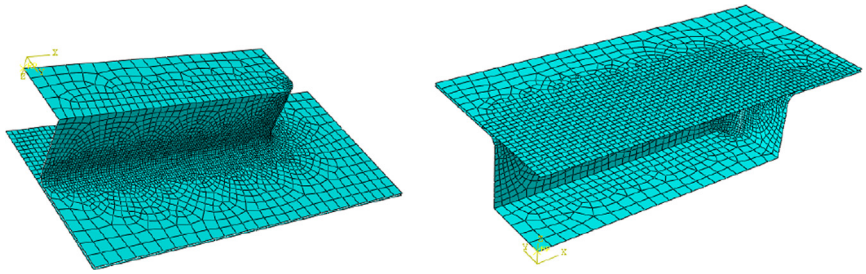

Fig. 10. One-quarter of the die and the sheet in ABAQUS EXPLICIT FEM environment.

seen from this figure, the predictions are in good agreement with experiments. The sheet center contact with the die after about 360 s. Fig. 13 shows the deformed sheet at that time and Fig. 14 compares the computed and predicted sheet thicknesses along its width at the contact time. In this figure predicted thicknesses from simulation without considering grain growth, is also added. In simulation without considering grain growth, grain growth coefficient, C set to be zero and other circumstances are the same as other simulations. As it can be seen in this figure if grain growth be ignored material flow stress reduces and predicted deformation is larger.

It can be seen from Fig. 14 that the predicted thicknesses are in good agreement with measured thicknesses, especially at the central zone where the friction coefficient does not affect sheet thickness. In the other word in this zone the most effective parameter on prediction accuracy is constitutive equation. Fig. 15 shows the tray after 840 s. At this instance, the corners of tray are also formed. Figs. 16 and 17 compare the predicted and measured tray thicknesses at that time in width and length directions respectively. In Fig. 16 predicted thicknesses from simulation without considering grain growth is also reported. Comparing Figs. 14 and 16, effect of considering grain growth is more obvious when the workpiece does not touch bottom of the die. Since at the end of the process workpiece shape is similar to the die, changing material flow stress due to grain growth does not affects final shape of the workpiece the same as the middle of the process.

These two figures also reveal that predictions by the model are in close agreement with experimental measurements. These results, obtained in this section prove that the model can well be used for various strain rates; stress states and when hardening due to grain size evolution exists.

Contribution of each deformation mechanism is distinguishable in all of the above simulations. The interested reader can refer

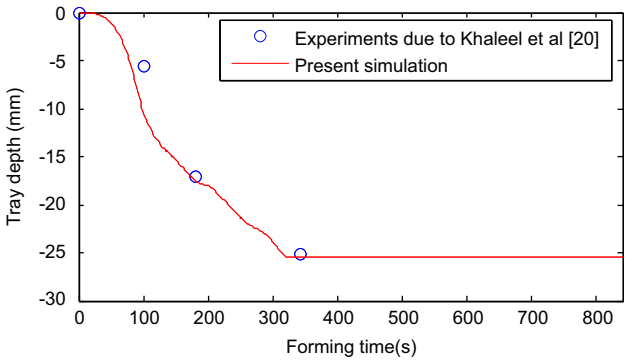

Fig. 12. Depth of the sheet center during forming vs. time.

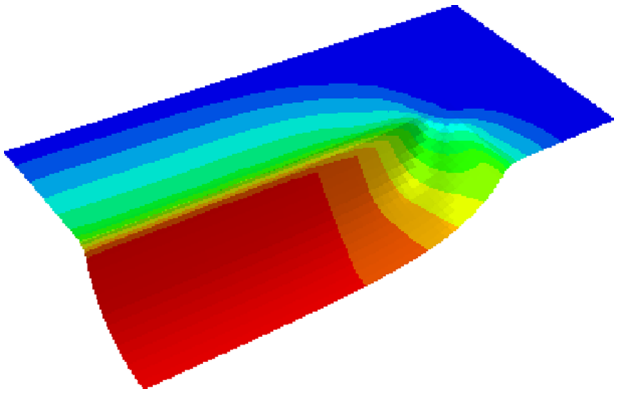

Fig. 13. Deformed sheet after 360 s.

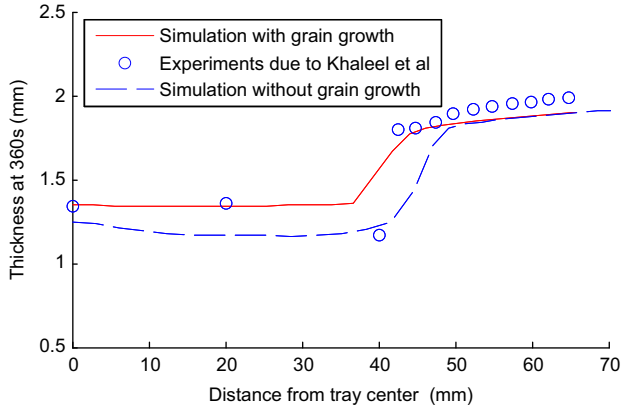

Fig. 14. Predicted and measured sheet thicknesses in width direction after 360 s.

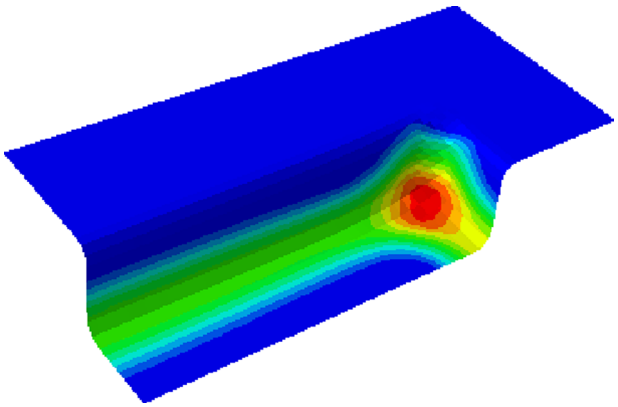

Fig. 15. Deformed sheet after 840 s.

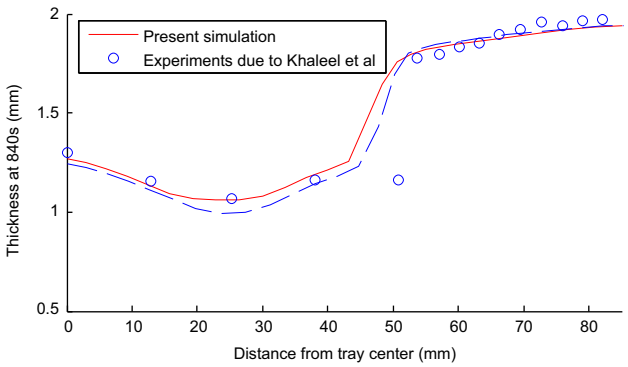

Fig. 16. Predicted and measured sheet thicknesses in width direction, after 840 s.

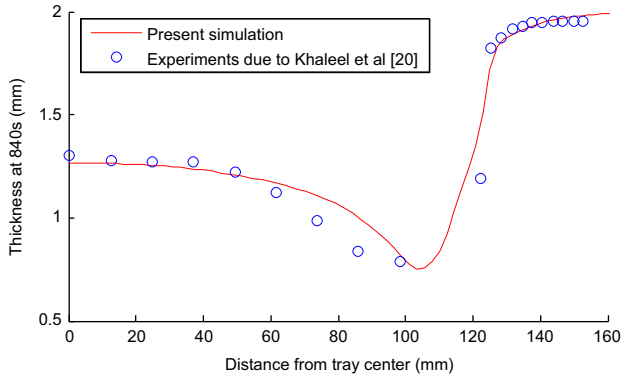

Fig. 17. Predicted and measured sheet thicknesses in length direction, after 840 s.

to Ref. [27] for more details. This capability of the models can help more understanding of the material deformation and observed phenomena.

5. Conclusions

In this paper, constitutive models are considered for inter-granular deformation and grain boundary mechanisms. Grain boundary mechanisms include: grain boundary sliding (GBS), grain boundary diffusion (GBD) and grain growth. Micro-constitutive models are proposed for GBS and GBD that correlate macro-stresses to strain rates.

Besides the above mentioned boundary mechanisms, inter-granular deformation is also predicted by three different approaches I: the Taylor type polycrystalline approach, II: Von-Mises viscoplastic model and III: a J2-J3 viscoplastic model.

It is shown that although model II and III perform much faster than model I and can be calibrated with less effort but they can well predict material behavior as accurate as model I. It is also shown that in different stress states, model III is closer to model I than model II.

The models were examined when hardening is also remarkable. It was revealed that the models can predict material behavior in various grain sizes, strains, strain rates and stress states. As an example of this situation a superplastic tray forming is simulated and compared with experimental observations.

Acknowledgments

The DB work was supported by the Romanian National University Research Council (CNCSIS), Program PCCE, Grant no. 6/2010.

References

[1] Chandra N. Constitutive behavior of superplastic materials. Int J Non-linear Mech 2002;37:461–84.
[2] Agarwal S, Briant C, Krajewski P, Bower A, Taleff E. Experimental validation of two-dimensional finite element method for simulating constitutive response of polycrystals during high temperature plastic deformation. J Mater Eng Perform 2007;16:170–8.
[3] Bower AF, Wininger E. A two-dimensional finite element method for simulating the constitutive response and microstructure of polycrystals during high temperature plastic deformation. J Mech Phys Solids 2004;52:1289–317.
[4] Cipoletti DE, Bower AF, Qi Y, Krajewski PE. The influence of heterogeneity in grain boundary sliding resistance on the constitutive behavior of AA5083 during high-temperature deformation. Mater Sci Eng: A 2009;504:175–82.
[5] Du N, Bower AF, Krajewski PE, Taleff EM. The influence of a threshold stress for grain boundary sliding on constitutive response of polycrystalline Al during high temperature deformation. Mater Sci Eng: A 2008;494:86–91.
[6] Kim JH, Semiatin SL, Lee CS. Constitutive analysis of the high-temperature deformation of Ti–6Al–4V with a transformed microstructure. Acta Mater 2003;51:5613–26.
[7] Langdon TG. A unified approach to grain boundary sliding in creep and superplasticity. Acta Metall Mater 1994;42:2437–43.
[8] Liu FC, Ma ZY. Contribution of grain boundary sliding in low-temperature superplasticity of ultrafine-grained aluminum alloys. Scr Mater 2010;62:125–128.
[9] Park SS, Garmestani H, Bae GT, Kim NJ, Krajewski PE, Kim S, et al. Constitutive analysis on the superplastic deformation of warm-rolled 6013 Al alloy. Mater Sci Eng: A 2006;435–436:687–92.
[10] Pan J, Cocks ACF. Computer simulation of superplastic deformation. Comput Mater Sci 1993;1:95–109.
[11] Hyde KB, Bate PS. Dynamic grain growth in Al–6Ni: modelling and experiments. Acta Mater 2005;53:4313–21.
[12] Rofman OV, Bate PS. Dynamic grain growth and particle coarsening in Al–3.5Cu. Acta Mater 2010;58:2527–34.
[13] Rabinovich MK, Trifonov VG. Dynamic grain growth during superplastic deformation. Acta Mater 1996;44:2073–8.
[14] Wilkinson DS, Cáceres CH. On the mechanism of strain-enhanced grain growth during superplastic deformation. Acta Metall 1984;32:1335–45.
[15] Cáceres CH, Wilkinson DS. Large strain behavior of a superplastic copper alloy – I. Deformation. Acta Metall 1984;32:415–22.
[16] Bontcheva N, Petzov G. Microstructure evolution during metal forming processes. Comput Mater Sci 2003;28:563–73.
[17] Kim B-N, Hiraga K, Sakka Y, Ahn B-W. A grain-boundary diffusion model of dynamic grain growth during superplastic deformation. Acta Mater 1999;47:3433–9.
[18] Yoshizawa Y-I, Sakuma T. Grain growth acceleration during high temperature deformation in high purity alumina. Mater Sci Eng: A 1991;149:59–64.
[19] Zhou M, Dunne FP. Mechanism-based constitutive equation for the superplastic behavior of a titanium alloy. J Strain Anal 1996;31:187–96.
[20] Khaleel MA, Johnson KI, Hamilton CH, Smith MT. Deformation modeling of superplastic AA-5083. Int J Plasticity 1998;14:1133–54.
[21] Khraisheh MK, Abu-Farha FK, Nazzal MA, Weinmann KJ. Combined mechanics-materials based optimization of superplastic forming of magnesium AZ31 alloy. CIRP Ann – Manuf Technol 2006;55:233–6.
[22] Ridley N, Bate PS, Zhang B. Material modelling data for superplastic forming optimisation. Mater Sci Eng A 2005;410–411:100–4.
[23] Nazzal MA, Khraisheh MK, Abu-Farha FK. The effect of strain rate sensitivity evolution on deformation stability during superplastic forming. J Mater Process Technol 2007;191:189–92.
[24] Filograna L, Racioppi M, Saccomandi G, Sgura I. A simple model of nonlinear viscoelasticity taking into account stress relaxation. Acta Mech 2009;204:21–36.
[25] Bonet J, Gil A, Wood RD, Said R, Curtis RV. Simulating superplastic forming. Comput Methods Appl Mech Eng 2006;195:6580–603.
[26] Krajewski PE, Hector Jr LG, Du N, Bower AF. Microstructure-based multiscale modeling of elevated temperature deformation in aluminum alloys. Acta Mater 2010;58:1074–86.
[27] Jafari Nedoushan R, Farzin M, Mashayekhi M, Banabic D. A microstructure-based constitutive model for superplastic forming. Metall Mater Trans A 2012;43:4266–80.
[28] Dawson PR, MacEwen SR, Wu PD. Advances in sheet metal forming analyses: dealing with mechanical anisotropy from crystallographic texture. Int Mater Rev 2003;48:86–122.
[29] Kuwabara T, Van Bael A, Iizuka E. Measurement and analysis of yield locus and work hardening characteristics of steel sheets wtih different *r*-values. Acta Mater 2002;50:3717–29.
[30] Roters F, Eisenlohr P, Hantcherli L, Tjahjanto DD, Bieler TR, Raabe D. Overview of constitutive laws, kinematics, homogenization and multiscale methods in crystal plasticity finite-element modeling: theory, experiments, applications, Acta Materialia;58: p. 1152–211.
[31] Inal K, Neale KW, Aboutajeddine A. Forming limit comparisons for FCC and BCC sheets. Int J Plast 2005;21:1255–66.
[32] Inal K, Wu PD, Neale KW. Finite element analysis of localization in FCC polycrystalline sheets under plane stress tension. Int J Solids Struct 2002;39:3469–86.
[33] Inal K, Wu PD, Neale KW. Instability and localized deformation in polycrystalline solids under plane-strain tension. Int J Solids Struct 2002;39:983–1002.
[34] Gawad J, Banabic D, Comsa DS, Gologanu M, Van Bael A, Eyckens P., et al., Evolving texture-informed anisotropic yield criterion for sheet forming, In: AIP Conference Proceedings of the 9th International Conference and Workshop on Numerical Simulation of 3D Sheet Metal Forming Processes; 1567 2013 p. 350–356.
[35] Schurig M, Bertram A, Petryk H. Micromechanical analysis of the development of a yield vertex in polycrystal plasticity. Acta Mech. 2007;194:141–58.
[36] Tugcu P, Neale KW, Wu PD, Inal K. Crystal plasticity simulation of the hydrostatic bulge test. Int. J. Plast. 2004;20:1603–53.
[37] Peirce D, Asaro RJ, Needleman A. An analysis of nonuniform and localized deformation in ductile single crystals. Acta Metall. 1982;30:1087–119.
[38] Peirce D, Asaro RJ, Needleman A. Material rate dependence and localized deformation in crystalline solids. Acta Metall. 1983;31:1951–76.
[39] Asaro RJ. Cryst. Plast. J. Appl. Mech. 1983;50:921–34.
[40] Asaro RJ, John WH, Theodore YW. Micromechanics of crystals and polycrystals, in: Advances in Applied Mechanics; Elsevier: 1983, p. 1–15.
[41] Huang Y. A user material subroutine incorporating single crystal plasticity in the ABAQUS finite element program. Massachusetts: Harvard University; 1992.
[42] Taylor GI. Plastic Strain in Metal. J Inst Met 1938;62:307–24.
[43] McNelley TR, Oh-Ishi K, Zhilyaev AP, Swaminathan S, Krajewski PE, Taleff EM. Characteristics of the transition from grain-boundary sliding to solute drag creep in superplastic AA5083. Metall Mater Trans A 2008;39:50–64.
[44] Kulas M-A, Green WP, Taleff EM, Krajewski PE, Mcnelley TR. Deformation mechanisms in superplastic AA5083 materials. Metall Mater Trans A 2005;36A:1249–61.
[45] Eric MT, Louis GH, John RB, Ravi V, Paul EK. The Effect of Stress State on High-Temperature Deformation of Fine-Grained Aluminum–Magnesium Alloy AA5083 Sheet 2009;57:2812–22.